Journal of Macromolecular Science®, Part C: Polymer Reviews, 45:99–124, 2005

ISSN 1532-1797 print/1525-609X online
DOI: 10.1081/MC-200055474

Taylor & Francis
Taylor & Francis Group

Focused Review

Study of the Molecular Mobility in Polymers with the Thermally Stimulated Recovery Technique—A Review

N. M. ALVES,[1,2] J. L. GÓMEZ RIBELLES,[3] AND J. F. MANO[1,2]

[1]Polymer Engineering Department, University of Minho, Guimarães, Portugal
[2]3B's Research Group—Biomaterials, Biodegradables, and Biomimetics, University of Minho, Braga, Portugal
[3]Center for Biomaterials and Department of Applied Thermodynamics, Universidad Politécnica de Valencia, Valencia, Spain

Thermally stimulated recovery (TSR) is a non-conventional mechanical spectroscopy technique that allows to analyse in detail the relaxation processes of polymeric systems in the low frequency region. This work reviews the main aspects and potentialities of this technique. The different kinds of TSR experiments that can be performed, global and thermal sampling (TS) experiments, are described and illustrated with several examples. Also, the different methods for the determination of the thermokinetic parameters (activation energy and pre-exponential factor) of the thermal sampling (TS) procedure are explained and compared. In this context, the compensation phenomenon, which always appears in TSR results when the studies are performed in the glass transition region of a given system, is discussed. Examples of the application of this technique to different polymeric systems during the last 20 years are provided. An emphasis will be made on the analysis of the effect of crystallinity degree and crosslink density on the TSR response. A comparison between the results (characteristic times and activation energies) obtained by different techniques, namely TSR, dynamic mechanical analysis (DMA), and differential scanning calorimetry (DSC), is made.

Keywords thermally stimulated recovery (TSR), non-conventional mechanical spectroscopy technique, global and thermal (TS) sampling experiments, thermokinetic parameters, compensation phenomenon, crystallinity degree, crosslink density, dynamic mechanical analysis (DMA), differential scanning calorimetry

Received 14 October 2004; Accepted 3 November 2004.
Address correspondence to J. F. Mano, 3B's Research Group—Biomaterials, Biodegradables, and Biomimetics, University of Minho, 4710-057 Braga, Portugal. E-mail: jmano@dep.uminho.pt

1. Introduction

Among the various available methods of analysing the relaxation processes and molecular motions of polymers are the so-called thermally stimulated techniques. They constitute an alternative to other conventional techniques such as dynamic mechanical analysis (DMA) or dielectric relaxation spectroscopy (DRS), offering the possibility to accede to lower frequencies ($10^{-3} - 10^{-4}$ Hz) associated with a high resolution. In thermally stimulated techniques a static stimulus is applied and the response is monitored while the sample is subjected to a temperature program, usually a heating at a constant rate. The most used of such techniques is the thermally stimulated depolarization currents technique (TSDC), where the polarization release of a previously poled sample is investigated. The first work related to this technique was published in the sixties (1) and other classical works related to this technique are listed in references (2), (3). In particular, a review of the various areas of application of thermally stimulated currents was made in reference (3). The corresponding mechanical equivalent technique is thermally stimulated recovery (TSR) and has also been used for more than 20 years (4–11), with the advantage of giving direct viscoelastic information and being used in non-polar systems. Moreover the study of conformational mobility with TSDC above T_g is usually masked by the presence of peaks associated with free charge mobility. However, TSR also present drawbacks such as the impossibility of investigating a material showing a significant irreversible flow response. A related technique, called creep rate spectroscopy, has also been reported (12, 13).

More recent works, where TSR is applied to the study of the temperature-dependent characteristics of materials, namely their phase transitions and molecular mobility, can be found in the literature, besides the classical works of references (4–11). Some examples are mentioned here: investigations of the α-relaxation dynamics in amorphous (14, 15) or semi-crystalline polymers (16, 17), copolymers or blends (18, 19) and thermosets (20, 21), studies of secondary relaxations (16, 22), analysis of the effects of humidity on the creep and recovery behavior of linear aliphatic nylons (23), characterization of the interface/interphase in composites (24, 25), and evaluation of the compatibility of different phases and phase separation in interpenetrated networks (26).

Recently, it was shown that TSR can also be used to perform physical aging studies (27). The characteristic parameters of the recovery upon heating were found to be sensitive to the evolution of structural relaxation (27). For two materials, a polyester thermoset and a semi-crystalline poly (ethylene terephthalate) (PET), and in all the aging temperatures studied, the TS characteristic parameters showed consistent variations with aging time, t_a: the activation energy decreased with increasing t_a and an opposite behavior was observed for the pre-exponential factor of the relaxation time τ_0 (see Equation (3) below). The decrease of the stored strain, ε_0, was related to the stiffening of the material upon aging. The shift of the process to lower temperatures, T_{max}, during structural relaxation was interpreted in terms of the shifting of the isolated retardation times towards lower values in the TS experiments.

TSR is usually designated in literature as thermally stimulated creep (TSCr) but in fact one should distinguish between TSCr and TSR experiments as shown in the next section. So this designation is related with the real principle of the experimental protocol: in global TSR experiments a static stress is imposed to the sample at a temperature (T_σ) higher than the temperature location of the relaxation under study. Thus, in the resulting strain all molecular processes are involved because all characteristic times, $\tau(T_\sigma)$, are small enough to quickly respond to the mechanical stimulus. During this mechanical

loading process the sample is cooled down to a lower temperature (T_0), at which the characteristic times are so high that any recovery process could not occur at a reasonable time scale.

The stress is eliminated at the temperature T_0. During a controllable heating process with no stress applied to the sample, those times are progressively reduced and when they reach sufficiently small values the recovery process may be observed as sudden decreases of the $\varepsilon(T)$ line (or peaks in a $d\varepsilon/dT$ plot).

By applying the thermal sampling (TS) or thermal windowing procedure described in Section 3, it is possible to decompose a complex process, characterized by a distribution of characteristic times, into narrow distributions of characteristic times, enabling analysis of the fine structure of the TSR global spectra (4–6, 8, 28, 29). For instance, the use of such procedure in the context of the TSR technique revealed that β relaxation processes in polyesters are a superposition of different contributions (30–32), allowed to resolve the overlapping processes at low temperatures of liquid-crystalline side-chain polymethacrylates (33) and revealed two components in the β retardation mode of some amine-cured epoxy networks (34) So, TSR constitutes a complementary tool to the DMA experiments. In fact, from dynamic measurements it is only possible to access the global behavior of the processes, whereas the TS procedure permits to experimentally decompose a complex process. Moreover, the low frequency character of TSR experiments and its non-isothermal character also allow extracting valuable information about the dynamics of the polymeric chains in less time than the typical isothermal mechanical creep/recovery experiments. In a previous work it was demonstrated that TSR can be performed in a commercial dynamic mechanical analyser (35), allowing to establish a better comparison between TSR and DMA data.

A description of the main aspects and potentialities of this non-conventional technique for clarifying the relaxation phenomena, and in particular the α-relaxation, is presented in this work. Several examples, in which the glass transition dynamics of distinct polymeric systems is analysed by TSR, will be given.

2. Global Experiments

The temperature-time programs of the two kinds of global thermally stimulated experiments that may be performed, thermally stimulated recovery (TSR) and thermally stimulated creep (TSCr), are schematically depicted in Figure 1. The response that results from the application of these two kinds of global experiments to a given system is complex, reflecting the existence of a distribution of retardation times. By applying such programs it is possible to monitor the recovery of the sample's strain as a function of temperature by TSR, whereas in TSCr it is the strain of a sample subjected to a static stress during a controlled heating that is measured as a function of temperature. It should be pointed out that performing a previous blank experiment (for each global or TS experiment) may be required to eliminate geometrical changes not assigned to the relaxational processes under study (35). A blank experiment is carried out under the same experimental parameters of the desired TS experiment but with no creep stress. It contains all the changes in a sample's geometry not resulting from the recovery process that one pretends to analyse.

An example of these two types of global experiments, conducted on a thermoset synthesized from a polyester resin based on orthophthalic acid, is given in Figure 2. This system showed negligible irreversible flow when subjected to mechanical stresses, which allowed to perform these experiments in the glass transition region (36). To our

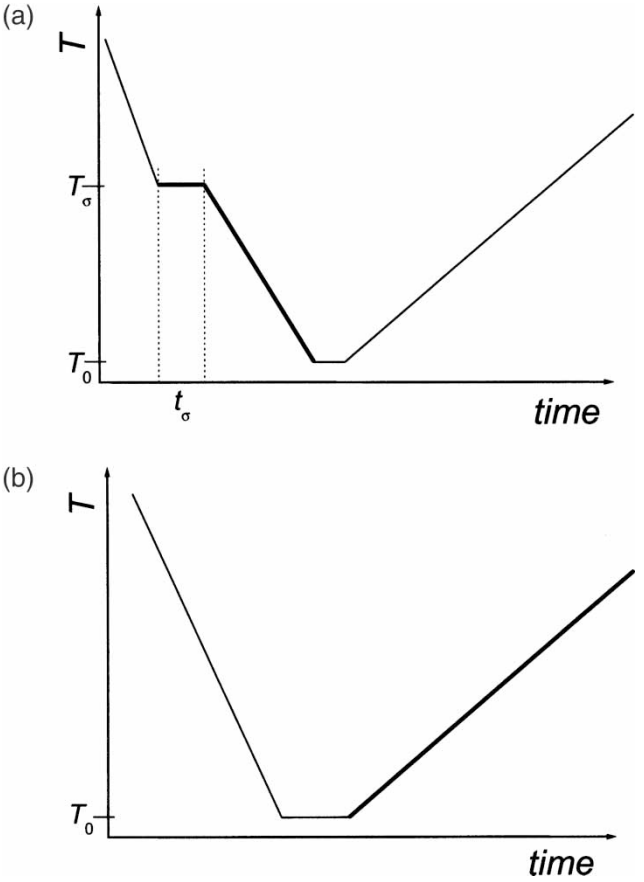

Figure 1. Temperature-time programs for global a) TSR and b) TSCr experiments. A static stress is applied during the steps with the thicker lines in the *T vs t* representation. The temperature T_σ is above the temperature range of the studied relaxation processes and t_σ is the creep time.

knowledge, this was the first time that TSR and TSCr results were presented simultaneously for a given material (36). The normalized derivative curves, $d\varepsilon/dT/(d\varepsilon/dT)_{max}$, were obtained through the numerical derivation of the previous data. Figures 2 and 3a clearly show the glass transition as an abrupt change in $\varepsilon(T)$ or as a peak in the $d\varepsilon/dT$ plot. The temperature of the maximum of $|d\varepsilon/dT|$, T_{max}, which can be seen as an indicative value of the glass transition temperature (T_g), is around 96°C, for both experiments. The general shape of the two peaks in Figure 3a is also very similar as we are probing the same molecular motions, i.e., micro-Brownian motions of the main chain segments with a similar time scale and both responses are governed by the retardation times.

The T_g of this sample was also measured by DSC (36), the most conventional technique to perform such analysis. This result is presented in Figure 3b in terms of the derivative of the heat flux in the temperature axis ($\partial Q/\partial T$). A peak is detected with a maximum at 97°C. This value corresponds to the temperature of the inflection point in the rise of the specific heat in the glass transition, that is one of the possible definitions

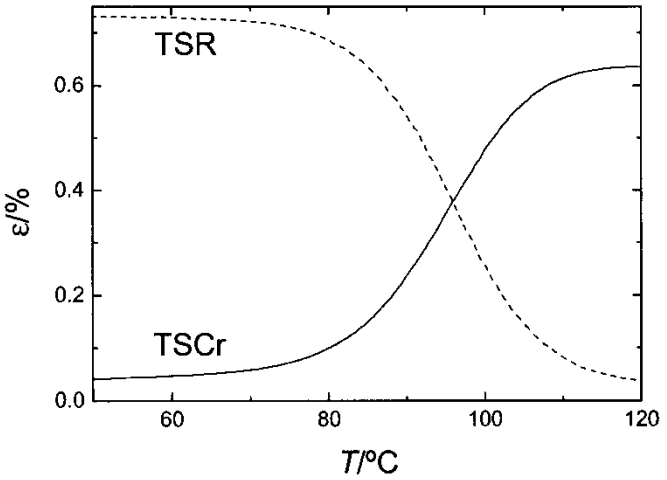

Figure 2. Global TSCr (solid line) and TSR (dashed line) spectra of a thermoset. The experimental conditions were, for both cases, $\sigma = 0.1$ MPa and $\beta = 4°C/min$. Data taken from reference (36).

of the calorimetric T_g. This temperature is generally close to the crossing point of the enthalpy lines corresponding to the liquid and the glass behaviors, i.e. the enthalpic glass transition temperature. The comparison between Figures 3a and 3b clearly show that T_{max}, measured by TSR and TSCr, and T_g, measured by DSC, are very similar, as expected for techniques with similar time scales. Small differences between such values could arise from the different thermal histories of the samples, namely the heating rate. So, T_{max} can be considered as a good parameter to characterize the glass transition.

TSR has been shown to be very sensitive to locate and characterize the glass transition of samples exhibiting crystallinity/orientation or crosslinking effects (37, 38) even when, in some cases, the T_g is not detectable by DSC (37). An example of this last statement is given in Figures 4 and 5 for an oriented and semi-crystalline PET. Although in a typical DSC scan at 10°C/min its T_g is almost undetectable (Figure 4), global spectra clearly revealed the α-relaxation between 100 and 110°C (Figure 5) (39).

3. Thermal Sampling (TS) Experiments

3.1. General Methodology

In these experiments the mechanical stress is applied only in a narrow temperature range within the temperature region where the global process appears. A typical TS experiment is schematically explained in Figure 6 and consists of the following steps: 1) a static stress σ_0 is applied at T_σ during a time period t_σ; 2) the sample is quenched to $T_r = T_\sigma - \Delta T_w$ with the stress applied; 3) the stress is removed and the mechanical strain is allowed to recover during a period of time t_r; 4) the sample is quenched to T_0, well below the temperature region of the global process (say 50°C below T_σ); and 5) the position of the probe tip, always in contact with the sample, is monitored during a controllable heating (typically 4°C/min), from T_0 up to a final temperature well above T_σ.

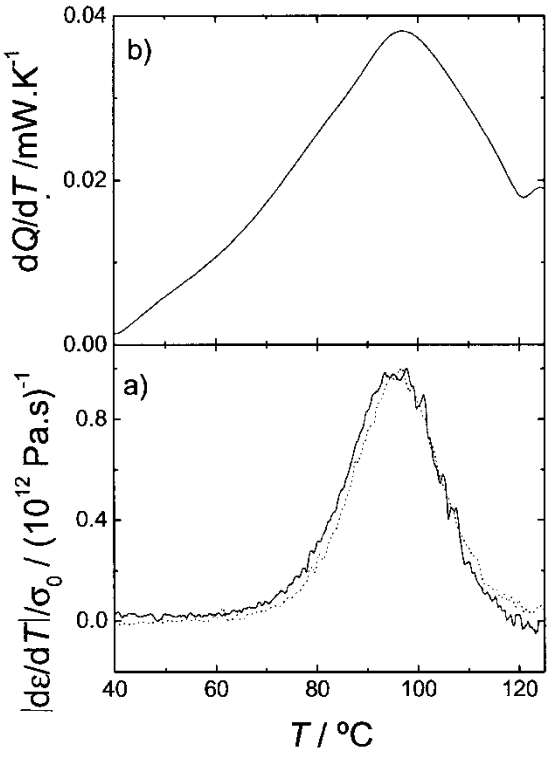

Figure 3. a) Normalized derivative of the lines shown in Figure 2 (solid line: global TSCR; dotted line: global TSR). b) Derivative of the DSC heat flux curve obtained on the studied thermoset at 10°C/min; prior to this experiment the sample was cooled from the equilibrium at 80°C/min down to 25°C. Data taken from reference (36).

With this procedure the purpose is to excite, as much as possible, a narrow distribution of characteristic times at a certain temperature from the broad spectrum of the entire process. It is possible to selectively fractionate the broad distribution of retardation times associated with the global process by performing different TS experiments at different T_σ, in the region of the complex relaxation process under study. Roughly speaking it can be said that the deformation of the sample in response to the applied stress σ_0 is due to the contribution of molecular groups that relax in times smaller than t_σ or that their retardation time is smaller than a characteristic retardation time τ_σ which depends on t_σ. Then, the temperature is decreased a few degrees to T_r and the stress made zero. Under these conditions the sample is kept for a time t_r and a part of the deformation is recovered, and this recovery is due to groups that at temperature T_r relax at times shorter than t_σ. Again, roughly speaking, it can be said that the remaining deformation of the sample at the end of this stage, and which will be monitored during heating, is due only to those molecular groups whose relaxation times are at T_σ shorter than t_σ but at the temperature T_r are longer than t_r. This selects a narrow window around τ_σ within the distribution of retardation times.

In a simple analysis, each TS curve can be identified with a thermally stimulated mechanical recovery process of an elementary mechanism. The Voigt-Kelvin model

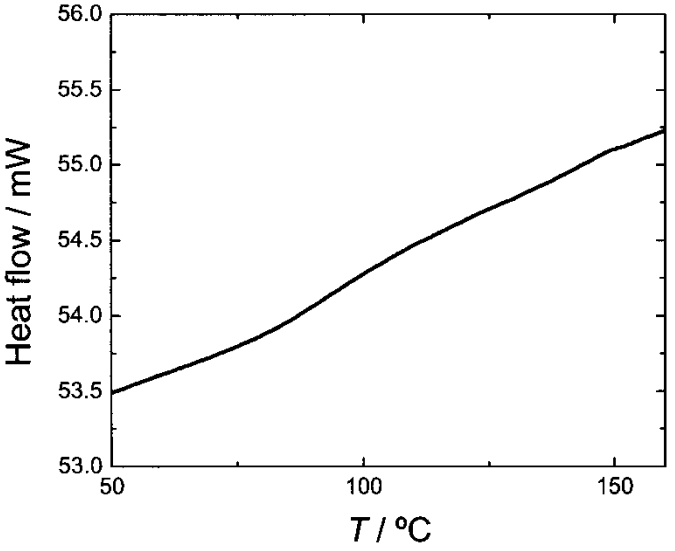

Figure 4. DSC heating scan at 10°C/min of a semi-crystalline PET ($X_c = 36\%$).

(parallel association of an elastic spring and a viscous dashpot) can be used in order to predict the dependence of the strain upon time or temperature. The corresponding constitutive equation is:

$$\tau(T)\frac{d\varepsilon(t)}{dt} = \frac{\sigma_0}{E} - \varepsilon(t), \tag{1}$$

where σ_0 is the static strain, E is the Young modulus of the spring element and $\tau(T)$ is the retardation time of the process. In the Voigt–Kelvin model the characteristic time is

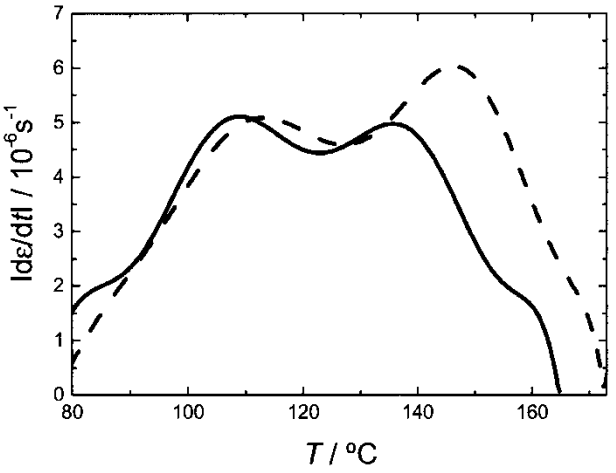

Figure 5. Global TSR spectra for the same PET of Figure 4. Solid line: $T_\sigma = 141.5$°C, dashed line: $T_\sigma = 151.7$°C. $\sigma_0 = 2$ MPa, $t_\sigma = 4$ min, $\beta = 4$°C/min. Data taken from reference (36).

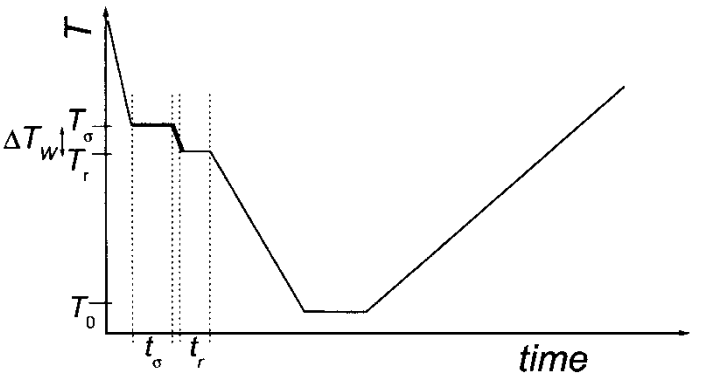

Figure 6. Temperature–time program of a TS experiment. The static stress is applied during the isothermal stage at and also during the cooling down to $T_\sigma - \Delta T_W$ (thicker lines). Typical values of the experimental variables: $t_\sigma \sim 5$ min, $\Delta T_w = T_\sigma - T_r \sim 3°C$, $t_r \sim 2$ min, $\beta \sim 4°C/\text{min}$. T_{max} is the inflexion temperature of $\varepsilon(T)$.

$\tau = \eta/E$, where η is the viscosity of the Newtonian dashpot. This model is equivalent to the Debye model used in the TSDC technique.

Applying Equation (1) to a mechanical recovery process ($\sigma_0 = 0$) during a heating at a constant rate $\beta = dT/dt$, the temperature dependence of the strain is

$$\varepsilon(T) = \varepsilon_0 \exp\left[-1/\beta \int_{T_0}^{T} dT'/\tau(T')\right], \tag{2}$$

where $\varepsilon_0 = \varepsilon(T_0)$.

Usually it is assumed that $\tau(T)$ obeys an Arrhenius type behavior,

$$\tau = \tau_0 \exp\left(\frac{E_a}{RT}\right) \tag{3}$$

and the two thermokinetic parameters characteristic of a TS experiment, the apparent activation energy E_a and the pre-exponential factor τ_0, are calculated based on the previous assumptions and equations.

In order to understand the influence of the experimental parameters chosen on the final TSR response, a systematic study was carried out by Alves et al. (40) for the three fundamental parameters of a TS experiment: the creep time t_σ, the window width ΔT_w, and the recovery time t_r. The use of a simple model to describe the TSR experiments on a system characterized by a distribution of activation energies allowed to predict the same variations detected in experimental TS results for a semi-crystalline PET in its glass transition region, when these parameters were independently changed: i) an increasing intensity of the TS peaks and a shift to higher temperatures as t_σ increases; ii) an increasing intensity of the TS peaks and a shift to lower temperatures as ΔT_w increases or t_r decreases (40). For this particular case it was concluded that the decrease of ΔT_w, usually considered the more obvious procedure to narrow the distribution of retardation times, was not the most efficient way to isolate a quasi-elementary process. For the studied system the decrease of t_σ seemed to be the most efficient strategy (40). Moreover, this work demonstrated that the change of any of the studied experimental

parameters could significantly affect the response of a material studied by TSR (40). In particular, the modification in the thermokinetic parameters (namely the activation energy) of the TS experiments may be very pronounced, especially if T_σ is close to but below T_g. So, the experiments performed on a material at different T_σ should use the same t_σ, ΔT_w and t_r values and the same should be applied when different materials are compared. These conclusions are also valid for TSDC.

Next, a summary of the main methods for calculating the thermokinetic parameters will be given. The activation energies of a semi-crystalline PET were calculated by the three methods that will be described here (35). It was found that the obtained activation energy is nearly independent on the method of calculation (35). In fact, all these methods are based on the modelling of the TS data with Equation (2). The good agreement between the methods may be an indication that this simple equation is a good description of the thermally simulated behavior of a quasi-elementary process, at least up to temperatures close to $T_{\max}$.

3.2. Determination of Thermokinetic Parameters

3.2.1. Bucci or BFG Method. From Equation (2) the creep rate $d\varepsilon/dt$ can be calculated:

$$\frac{d\varepsilon}{dt} = -\varepsilon_0 \tau^{-1}(T) \exp\left[-1/\beta \int_{T_0}^{T} dT'/\tau(T')\right]. \tag{4}$$

It can be easily found from Equations (2) and (4) that

$$\tau(T) = -\frac{1}{\beta} \frac{\varepsilon(T)}{d\varepsilon(T)/dT}. \tag{5}$$

Equation (5) is often applied for calculating the temperature dependence of the retardation time directly from the experimental results. This procedure, called the Bucci or BFG method, was first derived for the treatment of TSDC data (41). The calculation of $\tau(T)$ by the BFG method is carried out between $\sim T_{max} - 30$ and $\sim T_{max}$, where T_{max} is the temperature of maximum absolute creep rate. More detail in the use of Equation (5) can be found in reference (35).

3.2.2. Direct Fitting. Another way of obtaining the thermokinetic parameters is to directly fit the data to Equation (2). Three parameters are obtained for each TS curve: E_a, τ_0 and ε_0. Initial approximations of the ε_0 values are given by the $\varepsilon(T)$ values in the higher plateau of the experimental TS curves. The three adjustable parameters are obtained by minimization of the sum of square residues, S:

$$S = \Sigma_i[\varepsilon(T_i) - \varepsilon(T_i,\ \tau_0,\ E_a,\ \varepsilon_0)]^2, \tag{6}$$

by using a non-linear least-squares algorithm (Generalized Reduced Gradient),where $\varepsilon(T_i)$ are the experimental values and $\varepsilon(T_i, \tau_0, E_a, \varepsilon_0)$ are the theoretical ones, obtained from Equation (2). The fitting is conducted for values of $\varepsilon(T)$ between the initial higher plateau and approximately the temperature at the inflexion of the curve, covering typically a temperature range between 20 and 40°C.

It was shown that for each E_a value there is always a log τ_0 value that minimizes S, when the thermokinetic parameters are calculated through the direct fit method (42). The region of (log τ_0, E_a) that minimizes S is very deep, suggesting that the fitting of the data with a model assuming a single retardation time is an ill-posed problem (42). However, an

absolute minimum of S in the (E_a, $\log \tau_0$) plane, with coordinates compatible with the thermokinetic parameters obtained by other methods, should always be observed (35).

3.2.3. Initial-Rise Method. Another procedure that allows for the calculation of the thermokinetic parameters, which has been proposed for TSDC, is the initial-rise method (43). It is based on the fact that well below T_{max} the variation of the creep rate, $d\varepsilon/dt$, given by Equation (4), is mostly affected by the $\tau^{-1}(T)$ term, i.e., the exponential term can be considered as constant. Taking the Arrhenius behavior, one can write, under this assumption:

$$d\varepsilon/dt \sim -\exp(-E_a/RT). \tag{7}$$

From Equation (7) one can extract E_a from the slope of the linear regression of ln $(-d\varepsilon/dt)$ *vs* $1/T$. The pre-exponential factor, τ_0, may be obtained from the relationship between E_a, τ_0 and T_{max}:

$$\tau_0 \exp \frac{E_a}{RT_{\max}} = \frac{RT_{\max}^2}{\beta E_a}. \tag{8}$$

This equation is obtained by calculating the temperature of the maximum of the absolute creep rate variation by differentiation of Equation (4) and assuming an Arrhenius kinetics for the retardation time. It should be pointed that this equation is extremely important when using the TS procedure, because it relates to the three fundamental parameters that characterize a TS experiment (E_a, τ_0 and T_{max}). When this method is applied, the data used in the calculation range from temperatures at which the strain rate is ca. $(d\varepsilon/dt)_{max}/20$ and $(d\varepsilon/dt)_{max}/5$, where $(d\varepsilon/dt)_{max}$ is the maximum of strain rate (that occurs at $T = T_{max}$). Outside this data range a deviation from linearity is usually observed (35, 44). Note that as we are approaching $(d\varepsilon/dt)_{max}$ the initial assumption of this method is no longer valid.

3.3. Discussion of the Compensation Phenomenon

The Arrhenius lines of the TS curves obtained in the glass transition region but below T_g tend to converge to a single point (as can be seen, for instance, in Figure 9—see Section 3.4.1). This point is usually referred to in the literature as the compensation point, being characterized by a compensation temperature T_c and a compensation time τ_c. The compensation phenomenon has been extensively observed and discussed in the literature (8, 14, 33, 45, 46) and always appears in TSR and TSDC results when the studies are carried out in the glass transition region.

This compensation phenomenon can also be seen by a nearly perfect linear relationship between the thermokinetic parameters (E_a and $\log\tau_0$) when they are represented against each other (or equivalently by a linear relationship between the activation enthalpy and the activation entropy from the Eyring analysis (47, 48)). Figure 7 shows this compensation plot for several polymeric systems. Details about these materials and the experimental conditions can be found in Alves et al. (36–38, 49). The compensation parameters τ_c and T_c can be obtained from the linear fittings of the results presented in this figure:

$$\log \tau_{0,i} = \log \tau_c - E_{a,i}/\ln(10)RT_c, \tag{9}$$

where $\tau_{0,i}$ and $E_{a,i}$ are respectively the pre-exponential factor and the activation energy for the ith Arrhenius line.

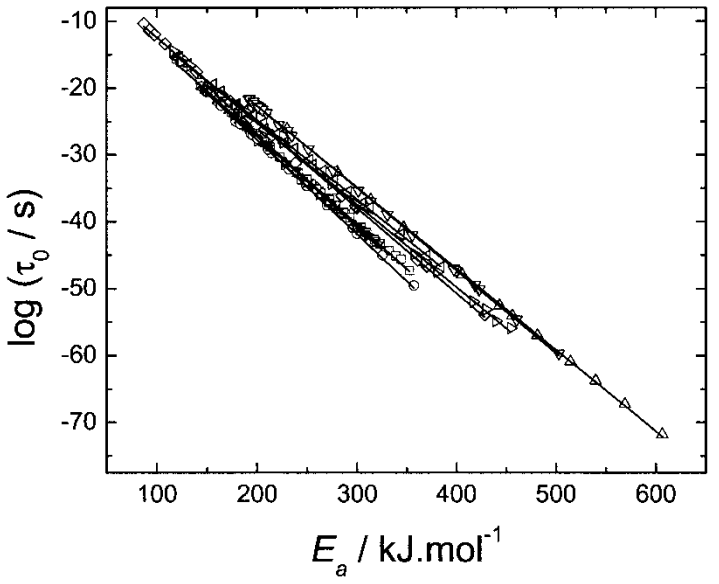

Figure 7. Compensation plot for several polymeric systems. (□) Biaxially oriented and semi-crystalline PET ($X_c = 36\%$) (PET2), (○) semi-crystalline PET ($X_c = 29\%$) (PET3), (Δ) PC (∇) short carbon-fiber reinforced PC, (◇) PMMA crosslinked with 0.5 wt% of EGDMA) (PMMA0.5), (◁) PMMA crosslinked with 5 wt% of EGDMA (PMMA5), (▷) PMMA crosslinked with 9 wt% of EGDMA (PMMA9) and (☆) polyester thermoset.

Substitution of this equation in the Arrhenius equation (Equation (3)) leads to

$$\ln \tau = \ln \tau_c + \frac{E_a}{R}\left(\frac{1}{T} - \frac{1}{T_c}\right) \tag{10}$$

known as the compensation law (6).

The compensation parameters are presented in Table 1 for the polymeric systems referred to in Figure 7.

For polycarbonate (PC) and short carbon-fiber reinforced polycarbonate (PC + CF) it was found that, despite the extensive overlap of the two linear representations, the compensation parameters are somewhat distinct. It may be interesting to notice that another study using TSR reported a higher compensation temperature and a lower compensation time for a composite system (an epoxy resin reinforced with glass beads) relative to the corresponding matrix (48).

For the polyester thermoset the compensation time is relatively low, compared with those observed in polymers with more flexible chains (49). A lower value of τ_c was

Table 1
Compensation parameters (τ_c and T_c) for the systems referred in Figure 7

	PC	PC + CF	Thermoset	PET2	PET3	PMMA0.5	PMMA5	PMMA9
T_c/°C	158	151	113	119	100	137	166	151
τ_c/s	27.5	90.6	0.6	0.3	2	1.8	0.1	0.3

also reported for a poly (cyanate epoxy) thermoset (21). From simulation of TSDC results it was also concluded that global peaks of systems obeying the compensation effect broaden as the compensation time decreases, for the same compensation temperature (50). This observation is consistent with the obtained results (Figure 3a) because the glass transition of this material is, in fact, broad when compared with the results observed in polymers with less stiff chains (49).

The model previously referred to for the simulation of TSDC data (50) is based on the assumption that the underlying processes may be described in terms of parallel (uncoupled) activated, Debye-like processes and was tested in several different polymer systems (51). It was found, for example, that for a side-chain liquid crystalline polymer the α-relaxation could be described by a Gaussian distribution function for the activation energy (with a mean value of $270\,\mathrm{kJ}\cdot\mathrm{mol}^{-1}$ and $\sigma = 130$) and with a compensation behavior with $\tau_c = 7.1\,\mathrm{s}$ and $T_c = 24.9^{\circ}\mathrm{C}$. Different TS experiments were simulated with $\beta = 4^{\circ}\mathrm{C/min}$ and the corresponding thermokinetic parameters were obtained by the BFG method (36). The knowledge of T_{max}, E_a and $\log \tau_0$ allowed for the representation of the temperature dependence of $\tau(T_{max})$ or equivalent frequency. The simulated results revealed the same trend usually obtained from experiments, i.e., the decrease of the retardation time with increasing T_{max} (36). From these results it was concluded that the slow increase of the equivalent frequency with temperature, always observed in TS experiments, is a natural consequence of the occurrence of a compensation effect in a system characterised by a distribution of characteristic times (36).

In Table 1 PET2 is a biaxially oriented and semi-crystalline film (crystallinity degree $X_c = 36\%$) whereas PET3 is an isotropic semi-crystalline material ($X_c = 29\%$). Unoriented and biaxially oriented films of PET have been compared for exploring the influence of molecular orientation and crystallinity on the compensation parameters (8, 52–54). However the results are not conclusive. In some studies there seems to be a variation of the compensation parameters with these factors (52, 54), reflected for instance in the decrease of τ_c with increasing crystallinity/orientation, whereas in another study (8) the influence is not significant. In these studies (8, 52, 54) T_c ranges between 5 and 30°C above T_g, as for the PET samples of Table 1. The decrease of τ_c, with increasing crystallinity/orientation, which also occurs for the PET samples in Table 1, was interpreted as a decrease of the size of the moving units (52).

In the case of the poly(methyl methacrylate) (PMMA) networks a systematic variation of the compensation parameters as the crosslinking degree increases was not observed. Different values can be found in literature for the compensation parameters of conventional uncrosslinked PMMA, e.g., $T_c = 164^{\circ}\mathrm{C}$ and $\tau_c = 1.6 \times 10^{-3}\,\mathrm{s}$ (47), $T_c = 155^{\circ}\mathrm{C}$ and $\tau_c = 0.01\,\mathrm{s}$ (55), or $T_c = 134^{\circ}\mathrm{C}$ and $\tau_c = 3\,\mathrm{s}$ (56). It is interesting to note that the values reported by Doulet et al. (56) are similar to those found in this work for the slightly crosslinked sample PMMA0.5 (the number after PMMA refers to the mass fraction of the crosslinking agent: ethylene glycol dimethacrylate - (EGDMA)). It has also been reported for PMMA that T_c is sometimes more than 50°C above T_g (55) and that T_c, contrary to τ_c, is dependent on tacticity (56).

In fact, the practical significance of the compensation parameters appearing in thermally stimulated studies is difficult to interpret and up to now no consistent theory has offered an unambiguous explanation for their physical origin. Various interpretations of the compensation phenomenon can be found in the literature, e.g., it has been considered as an indicator of cooperative molecular motions or some other cooperative transitions (48, 53, 57–59), explained in terms of the coupling model by Marchal (60, 61), who suggested that T_c could be related to a phase transition temperature (57, 62), or

explained as an information transfer between the two thermokinetic parameters by means of some kind of thermal mechanism (63, 64). The difference between T_c and T_g has been related to the stiffness of the polymeric chain (8), though this relation is not very clear as shown by Ramos et al. (65). Some authors have argued that this phenomenon does not have a true physical origin but rather it is a result of statistical error propagation (66). However, in some cases (67, 68) this phenomenon could not be simply described by an error propagation. It was suggested that the compensation phenomenon cannot be considered as a basic feature of the glass transition relaxation but that it is just a mathematical consequence of a fundamental relationship between the Gibbs energy and temperature (65). Another argument supporting the lack of a physical basis for this phenomenon is that it predicts that at the compensation temperature, usually observed 5–30°C above T_g for the generality of materials (56, 65), all the characteristic times of the different processes are the same; this means that at T_c the system behaves as an elementary process. Of course this is not an acceptable possibility in the case of most polymeric systems. In fact, the existence of a distribution of characteristic times at T_c was demonstrated for an isotactic polypropylene (69) and for a semi-crystalline PET (70), both studied by mechanical spectroscopy techniques.

The results presented in Figure 7 also seem to indicate that the compensation phenomenon is, in fact, a pure mathematical consequence of the underlying process and does not have a true physical origin, because it is seen for completely distinct polymeric systems (e.g., unreinforced and reinforced amorphous thermoplastic, semi-crystalline thermoplastics with different crystallinity and orientation, a thermoset, and polymer networks with variable crosslinking degree) that the compensation lines tend to converge to the same point. It seems independent of important factors such as reinforcement, crystallinity, orientation, or crosslinking. In addition, it was previously found that compensation is independent on the previous thermal history below T_g undergone by the material (37).

A recent work has given further arguments for attributing the compensation effect to a pure mathematical consequence of the underlying process (42) This work has shown that there is an intrinsic compensation between the two thermokinetic parameters in the description of the TS data, when the direct fitting method is used to calculate E_a and $\log \tau_0$ (42). This conclusion was based on the observation that for each E_a value there is always a $\log \tau_0$ value that minimises S (42). This fact is also responsible for the valley shape of the S plot (42). It was shown that the temperature dependence of the strain ε during a heating experiment may be simplified by $\varepsilon(T) \propto \exp[-c/\tau(T)]$, where c is a constant and $\tau(T)$ is the Arrhenius retardation time (42).

It was also found that compensation coordinates obtained from different sets of the same original collection of ($\log \tau_0$, E_a) correlate themselves (42). If one isolates the best compensation points, a perfect linear relationship is obtained. This effect, reported for the first time in TSR results, was designated as hyper compensation (42).

3.4. Examples of the Application of the TS Procedure to the Study of the Glass Transition Dynamics of Polymeric Systems

3.4.1 Effect of Crystallinity. The semi-crystalline morphology of a polymer introduces a confinement of the glass-forming regions at the nanometer scale, which obviously influences the α-relaxation associated to the glass transition. So, the glass transition of a semi-crystalline polymer is dependent on the crystalline fraction and also on its microstructure (71–74).

PET can be easily obtained either as closely amorphous or with a crystallinity degree that can vary from ~0 to 50%, as a result of thermal treatments above the glass transition (75, 76). Uniaxial or biaxial drawing could also induce the formation of a crystalline phase in the amorphous material (77, 78) and for example, for high values of uniaxial drawing the effect is more to align the crystallites with the drawing direction rather than to increase the degree of crystallinity (79). These facts demonstrate that PET is suitable material to be investigated with different crystallinity and orientation profiles.

TS experiments were performed in the glass transition region of two different PET samples: PET3, an isotropic bar with a crystallinity degree X_c of 29% and PET2, a biaxially oriented film with $X_c = 36\%$ (37). Figure 8 shows some of those experiments represented in terms of the absolute derivative of the measured strain recovery as a function of temperature. These curves show a peak with the maximum appearing at $T = T_{max}$ and are shifted to higher temperatures as T_σ increases. For $T \leq T_g$, the height of the peak increases as T_σ increases due to the progressive activation of more molecular groups participating in the relaxation process for a given time, as is typically seen in this kind of experiment (36, 49). Similarly, TS results from TSDC experiments in the glassy state, exhibit an increase of the total polarization with increasing polarization temperature towards T_g (see, for example references (57, 67, 80)). Above T_g the height tends to stabilize and usually a decrease is observed above the temperature at which the activation energy begins to decrease. This occurs because the retardation times become smaller as the temperature goes to the elastomeric plateau and the relaxation modes in the region of TSR (~100 s) become more scarce (70). The intensity of the peaks is lower for PET2 than for PET3 reflecting a more crystalline/oriented sample with a smaller amorphous phase and hence with a less intense α-process. The decrease of the peak area with increasing orientation was also detected by TSDC (81) for PET samples with different drawing ratios (from 1 to 7.2).

The Arrhenius plots for the two samples, obtained by applying the BFG method to the previously shown experimental results, are presented in Figure 9 (37). The obtained variation of the activation energy with temperature is shown in Figure 10 for the two samples (37). The high values of E_a usually obtained for the TS experiments carried out in the glass transition region may be explained on the basis of cooperative conformational rearrangements of the macromolecular segments. A nearly constant value of E_a is obtained at low temperatures for PET2, which may be explained by the Adam-Gibbs theory that states an Arrhenius behavior for the chain mobility in the glassy state when the configurational entropy becomes independent of temperature (82). E_a presents a maximum at a temperature around T_g, where the change from the Arrhenius to the VFTH regimes occurs. So, the temperature of the maximum activation energy can also be used to locate the glass transition of the sample. This change from an Arrhenius to a VFTH behavior has also been observed by low-frequency dielectric spectroscopy (83) and TSDC techniques (84). Above T_g the materials are in thermodynamic equilibrium and E_a decreases as the temperature gets higher, according to the VFTH equation (70).

The maximum values of E_a obtained in this work (37), 354 kJ/mol for PET2 and 388 kJ/mol for PET3, are in agreement with the one found in the literature for semi-crystalline PET by thermally stimulated depolarization currents (TSDC) (≈378 kJ/mol) (45), while for amorphous PET the maximum value of E_a is usually higher (≈457 kJ/mol) (45).

Different profiles of variation of E_a with temperature and different values of E_a at the transition from the Arrhenius to the VFTH behavior were obtained for these PET samples with different crystallinity and orientation (37), as can be seen in Figure 10. PET2 has a

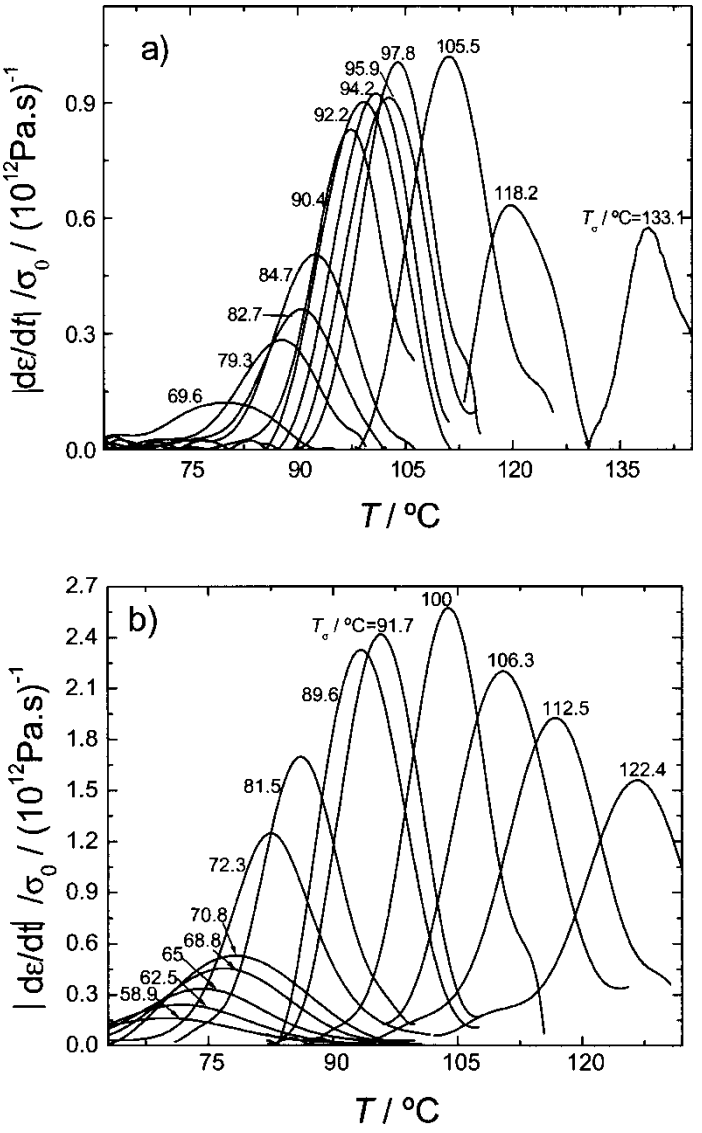

Figure 8. Absolute derivative of the measured strain recovery as a function of temperature for a) PET2 and b) PET3. The experimental conditions were $\beta = 4^\circ C/min$, $\Delta T_W = 3^\circ C$, $T_0 = T_\sigma - 50^\circ C$, $t_\sigma = t_r = 4\,min$ and $62.1^\circ C < T_\sigma < 136.1^\circ C$ for the film and $58.9^\circ C < T_\sigma < 122.4^\circ C$ for the bar. For clarity not all the performed experiments are plotted. Data taken from reference (37).

lower activation energy than PET3. According to Sauer and Kim (85) the lower values of E_a are an indication that the polymer chains are more homogeneous in terms of their structural regularity and/or composition. The lower values of E_a exhibited in Figure 10 by the oriented semi-crystalline PET were attributed to its higher structural regularity when compared with the isotropic semi-crystalline PET (37). The T_g of PET2 (107°C), estimated by TSR as the temperature of the maximum activation energy (Figure 10) is $\approx$12°C higher than the T_g of PET3 (95°C).

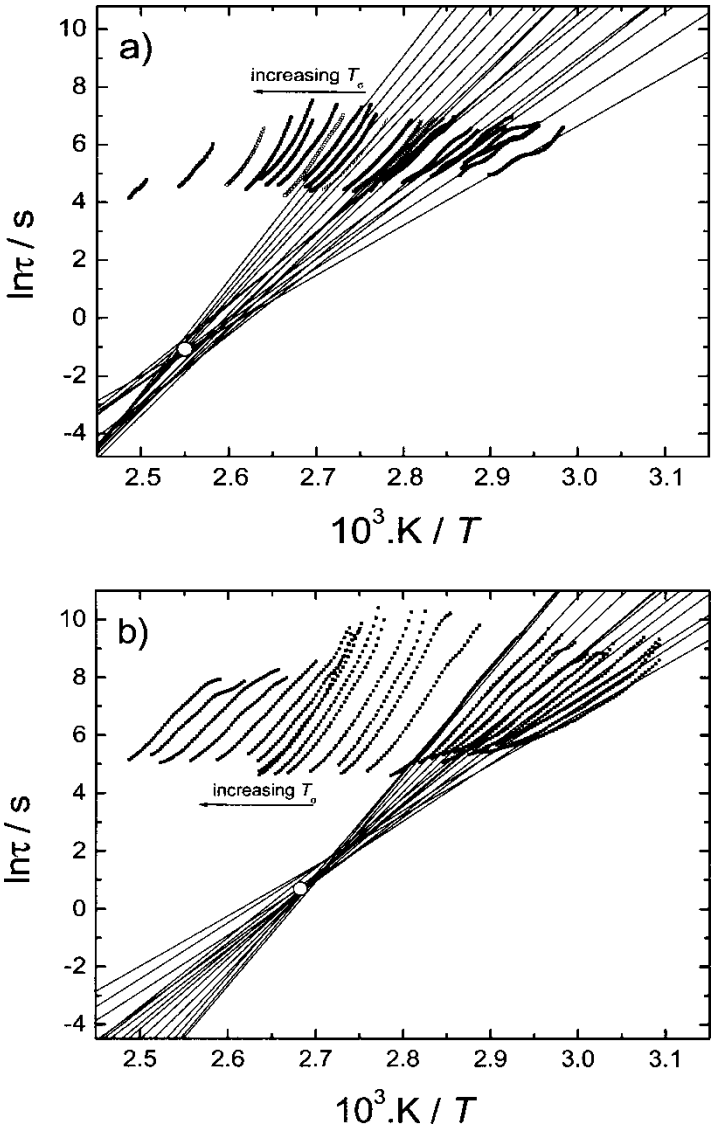

Figure 9. (□) TS data in the glass transition region. a) PET2; b) PET3. In the glassy state the Arrhenius lines (solid lines) converge to the compensation point (circle) (this issue is discussed in Section 3.3). Data taken from reference (37).

3.4.2. Effect of Crosslink Density. The segmental dynamics of polymeric systems is strongly affected by intermolecular constraints (86, 87). The crosslinks of a polymer network constitute a way of constraining the segmental motions, and, in many cases, play a similar role as entanglements in linear polymers with sufficiently high molecular weight. The effect of crosslinking degree on the α-relaxation has been investigated by several authors and revealed a significant broadening of this relaxation and a slowing down of the segmental dynamics as crosslink density increases (88–91). The behavior of non-crosslinked PMMA in the glass transition region has been extensively studied by

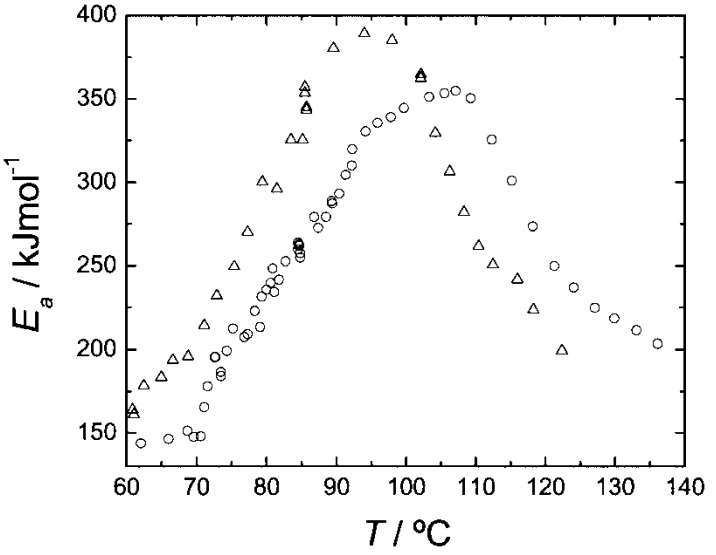

Figure 10. Activation energies as a function of temperature for PET2 (open circles) and PET3 (open triangles) calculated in both the glassy and equilibrium states from TS experiments. Data taken from reference (37).

various techniques (e.g., references (92, 93)), which makes this amorphous polymer a suitable system to investigate and improve the comprehension of the crosslinking effect on the α-relaxation. The segmental dynamic behavior of PMMA has been studied by thermally stimulated methods, primarily by thermally stimulated currents (14, 85, 94–97). Also, some works of thermally stimulated creep can be found (14, 56). Recently, the effect of crosslinking degree on the α-relaxation of PMMA was investigated by TSR (38), using ethylene glycol dimethacrylate (EGDMA) as the crosslinking agent. TS results obtained for PMMA networks with different crosslinking degrees, in the glass transition region, can be found in reference (38). An example of such results is shown in Figure 11, for PMMA crosslinked with 0.5% by weight of EGDMA. The shift of the curves to higher temperatures and the increase of the low temperature plateau of the TS curves as T_σ increases are shown.

The thermokinetic parameters were calculated with the BFG method for the three samples (38). The variation of E_a with T_σ for the three samples is presented in Figure 12. The transition from an Arrhenius to a VFTH behavior, presented in the previous section for PET, was also observed for these PMMA networks (38). For all the samples it was possible to obtain E_a at quite low temperatures, far below T_g. In this temperature range E_a depends only slightly on temperature, adopting an Ahrrenius behavior characteristic of the glassy state.

The degree of cooperativity of an observed process can be analysed by observing the deviation of the activation energy relative to the zero-entropy case (98). Starkweather suggested that localized processes should occur with negligible activation entropy. In this case the activation energy can be given by,

$$E_a = RT[1 + \ln(k_B T/2\pi hf)]. \tag{11}$$

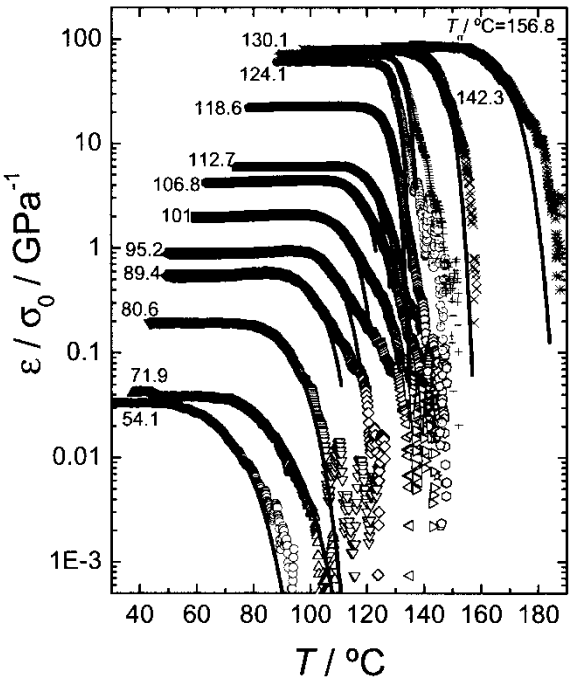

Figure 11. TS results in the glass transition region for PMMA with 0.5 wt% of EGDMA, obtained at different creep temperatures T_σ (in the graphics). The solid lines are the simulated curves with the thermokinetic parameters obtained from the Arrhenius fitting of the $\tau(T)$ results. Data taken from reference (38).

where f is the frequency of the experiment, k_B is the Boltzmann constant and h is the Planck constant. In TSR experiments the equivalent frequency, f, can be assumed to be $\sim 10^{-2.5}$ Hz; this value was based on the observation of numerous thermally stimulated depolarization results (99).

Lacabanne and co-workers used the Starkweather procedure previously described and showed that even at low temperatures, far below T_g, the involved motions in PMMA are still cooperative (14). Such behavior seems to be quite general, as it was also found at low temperatures for other polymeric systems (36, 49, 100).

The same features in $E_a(T)$ described here for PMMA were observed by thermally stimulated depolarization currents (TSDC) (e.g. references (14, 85, 97)). The values of maximum E_a obtained by TSR in this study (38) were similar to the ones found in the literature for uncrosslinked PMMA by thermally stimulated creep (14) and TSDC (47). Also, the temperatures of maximum E_a obtained by TSDC ($\approx$120°C) (101) for uncrosslinked conventional PMMA, using the TS procedure, is similar to the one found here by TSR for the slightly crosslinked sample ($\approx$127.2°C) (38), although the last value is somewhat higher due to the presence of EGDMA.

These results showed that the profile of variation of E_a with temperature, obtained through the TS procedure, is sensitive to crosslinking effects: a significant shift of the α-relaxation to higher temperatures as well as a broadening of the process as the crosslinking degree increases was observed (38). The broadening of the α-relaxation as the EGDMA content increases is due to the increase of molecular environments felt by the

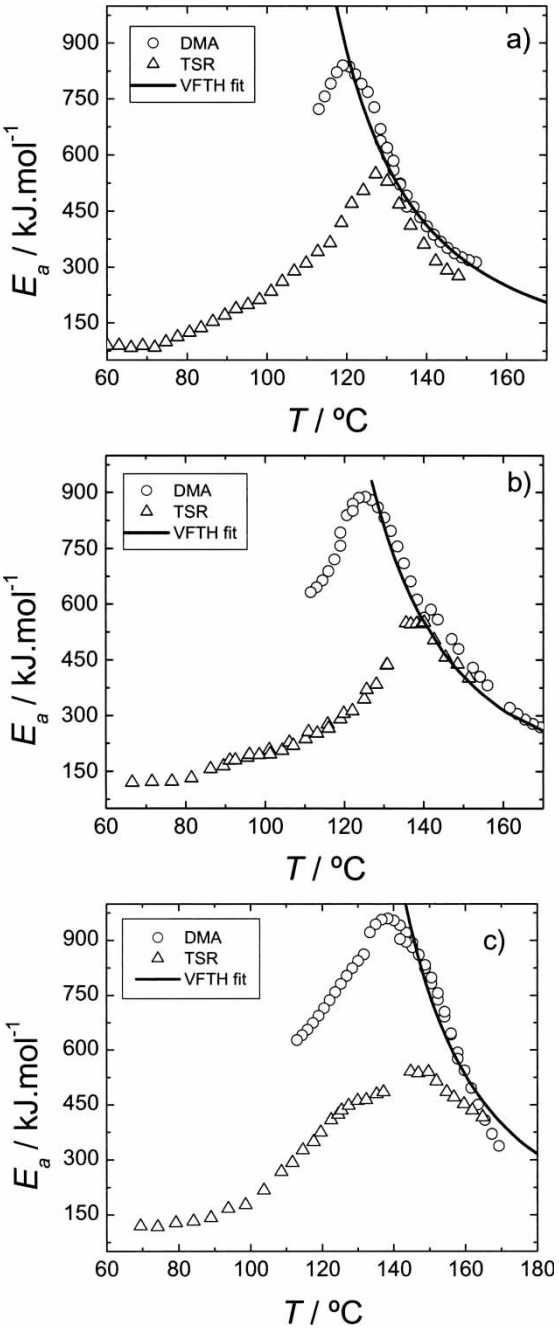

Figure 12. Temperature dependence of the apparent activation energy across the glass transition for a) PMMA with 0.5 wt% of EGDMA, b) PMMA with 5 wt% of EGDMA and c) PMMA with 9 wt% of EGDMA. ○-DMA results, calculated from the temperature shift factors (numerical differentiation). By fitting the shift factors in the liquid state with the WLF equation and using the relations between the WLF and VFTH parameters $E_a(T)$ curves were computed with the corresponding B and T_2 parameters (solid lines). △-TSR results, where E_a was obtained from the TS curves by applying the BFG method and assuming an Arrhenius behavior. Data taken from reference (38).

segmental motions, imposed by the crosslinks. A variation of T_g with crosslinking degree of about 20°C from the slightly crosslinked PMMA to the more crosslinked sample and a transition between a VFTH and a Arrhenius behavior is observed both by DMA and TSR (Figure 12). Above T_g, the E_a values obtained from DMA, and TS experiments agree very well.

3.5. *Comparison Between TSR, DMA and DSC Results*

The activation energies as a function of temperature obtained by TSR and DMA, calculated for distinct PMMA networks in a previous work (38) and shown in Figure 12, were compared with the activation energy values obtained by creep for the same networks (38). It was found that the transition from the Arrhenius to the VFTH regime can be detected by DMA, creep, and TSR (38). The main difference is that TSR allows to characterize the relaxation features in the glassy state more accurately. In fact by TSR the activation energy can be obtained at very low temperatures, as seen in Figure 12. In the TSR experiments the transition from the Ahrrenius to the VFTH behavior is shifted towards higher temperatures and the maximum E_a is lower with respect to the DMA (Figure 12) or creep data (38) due to the isothermal character of DMA and creep experiments (102).

The variation of the characteristic times with temperature obtained for a semicrystalline PET and by different techniques (70) is shown in Figure 13. The times $\tau(T_{max})$ as a function of T_{max} obtained for different TS curves are often a measure of

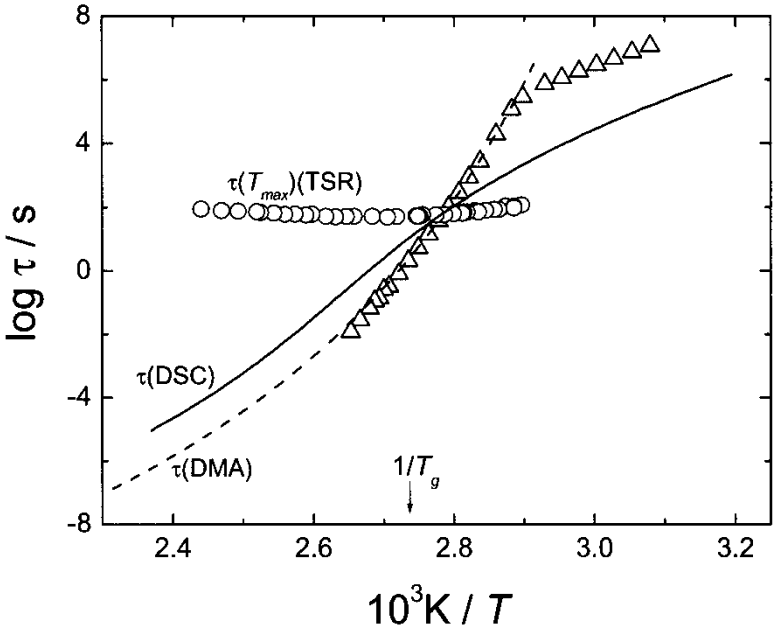

Figure 13. Circles: retardation time at the inflexion temperature of the TS curves (T_{max}) as a function of T_{max} for the studied PET. Triangles: mean retardation times as a function of temperature calculated from DMA experiments; the dashed line linked to these data is an extrapolation to higher temperatures according to the VFTH equation. Solid line: mean retardation times as a function of temperature obtained from DSC. More details can be found in reference (70, 103).

the time scale of TS experiments due to the fact that at that temperature the variation of the strain during the recovery process is maximum. It is seen that these retardation times do not vary significantly on the logarithmic axis, taking values near 100 s, such as in TSDC experiments (99). The magnitude of these values is also typical for DSC time scales.

The mean retardation times calculated from DSC experiments through application of a configurational entropy based model (103) are also presented in Figure 13. It can be seen that above T_g the DSC and DMA lines are approximately parallel and the DSC times are higher than the DMA times. Although the same physical phenomenon (conformational rearrangements in the glass transition region) is analysed, the measured properties and the type of solicitation are distinct; hence, the DSC and DMA times at a given temperature should not be necessarily the same, which in fact was observed. It should be noted that in the glassy state it is not correct to directly compare DSC and DMA data, because both experiments are performed under very distinct thermal histories. The DSC curve corresponds to a cooling experiment at $40^{\circ}C/min$ whereas the DMA data results from isothermal experiments, where the sample stayed $\sim$20 min at each temperature. The transition from the glassy state to the equilibrium phase is detected by both DSC and DMA in Figure 13. Well below T_g a typical Arrhenius behavior is detected from the linearity between log τ and $1/T$. Above T_g a clear curvature on the relaxation plot is visible, which can be well described with the VFTH Equation (70).

This comparison between DMA and TSR results demonstrates the complementary character of both techniques. It can be concluded that the molecular mobility is studied by TSR in a narrow time scale range when compared with DMA, but at low frequencies, below the usual frequency range covered by typical DMA experiments.

Figure 14 compares the activation energies obtained by TSR, DSC and DMA for the same PET of Figure 13 (70). The E_a values corresponding to the TS experiments were calculated by applying the BFG method and are plotted here as a function of T_{max}.

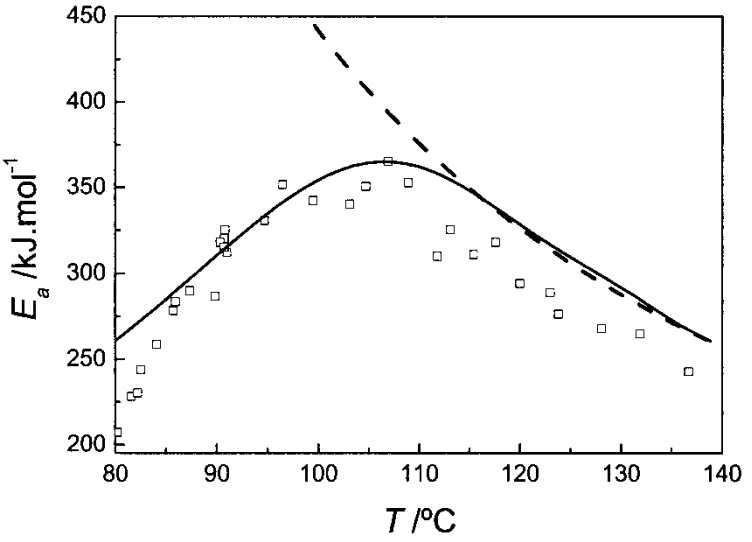

Figure 14. Activation energies as a function of temperature calculated in both the glassy and equilibrium states from TSR (squares) and from DSC experiments (solid line). The dashed line is the activation energy calculated from the DMA results in the equilibrium state, using the VFTH equation. More details can be found in reference (38).

The apparent E_a values corresponding to DSC were obtained from differentiation of the data shown in Figure 13. The dashed line corresponds to the activation energy values calculated from the DMA results in the equilibrium state.

It was found that the transition from an Arrhenius behavior characteristic of the metastable glassy state and a typical behavior of a liquid in equilibrium can be detected either by TSR and DSC (70). Interestingly enough, a good agreement is found between DSC and TSR values in Figure 14. The E_a maximum occurs at the same temperature in the two techniques, which have similar equivalent frequencies. Also, for $T > T_g$ the DMA results are in accordance with the ones obtained by TSR and DSC.

4. Final Comments

In general it can be said that the non-conventional technique, TSR, constitutes an important tool for the analysis of the molecular mobility of polymeric systems and complements the information obtained by other more common techniques such as DMA, DSC, creep or DRS. Its principal advantages are the possibility of acceding to lower frequencies (10^{-3}–10^{-4} Hz), associated with a higher resolution and, by applying the TS procedure, the ability to decompose a complex process, characterized by a distribution of characteristic times, into narrow distributions of characteristic times. Due to its high sensitivity, the TSR technique is also adequate for identifying glass transition (or secondary relaxation) processes, especially in systems where this task is not straightforward by conventional techniques (e.g. DSC), such as thermosets or highly crystalline polymers. The impossibility of investigating a material that presents a significant irreversible flow response constitutes its major drawback. Moreover, it must be pointed out that there is still a need for improving the modelling of the TSR response. This is particularly relevant for the description of the glass transition process where structural relaxation is neglected in the mathematical description of the TSR experiments.

Appendix: List of Symbols and Abbreviations

B	parameter of the VFTH equation
BFG	Bucci-Fieschi-Guidi (method)
DMA	dynamic mechanical analysis
DSC	differential scanning calorimetry
DRS	dielectric relaxation spectroscopy
E	Young modulus of the spring element of the Voigt-Kelvin model
E_a	apparent activation energy given by the Arrhenius formalism
EGDMA	ethylene glycol dimethacrylate
PC	polycarbonate
PC + CF	short carbon-fiber reinforced polycarbonate
PET	poly(ethylene terephthalate)
PMMA	poly(methyl methacrylate)
R	ideal gas constant
S	sum of square residues (Eq. (6))
T_c	compensation temperature
T_g	glass transition temperature

T_{max}	temperature at which the variation of strain is maximum during a TSR experiment
T_0	minimum temperature of a TSR experiment at which the characteristic times are very high
T_2	parameter of the VFTH equation
T_σ	creep temperature at which σ_0 is applied during t_σ
TS	thermal sampling
TSCr	thermally stimulated creep
TSDC	thermally stimulated depolarization currents
TSR	thermally stimulated recovery
VFTH	Vogel-Fulcher-Tamman-Hesse (equation)
WLF	Williams-Landel-Ferry (equation)
X_c	degree of crystallinity
f	frequency of the experiment
h	Planck constant
k_B	Boltzmann constant
t_a	ageing time
t_r	recovery time
t_σ	creep time
ΔT_w	temperature interval where σ_0 is applied during a TSR experiment. For a global experiment $\Delta T_w = T_\sigma - T_0$ and for a TS experiment ΔT_w is typically 2–3°C
β	heating rate (dT/dt)
ε	strain
ε_0	strain in a TSR experiment at the beginning of the heating process (at T_0)
σ_0	static stress applied during a TSR experiment
η	viscosity of the Newtonian dashpot of the Voigt-Kelvin model
τ	retardation time
τ_0	pre-exponential factor of the Arrhenius equation
τ_c	compensation time

Acknowledgements

Financial support for this work was provided by FCT, through the POCTI and FEDER programmes. JLGR wish to acknowledge the support of the Spanish Science and Technology Ministry through the MAT2001-2678-C02-01 project.

References

1. Bucci, C. and Fieschi, R. (1964) *Phys Rev. Lett.*, 12: 16.
2. (a) van Turnhout, J. and Polymer, J.1971, 2: 73; (b) van Turnhout, J. (1975) *Thermally Stimulated Discharge of Polymer Electrets*. Elsevier: New York.
3. Lavergne, C. and Lacabanne, C. (1993) IEEE Electrical Insulation Magazine 9: 5.
4. Chatain, D., Gautier, P.G., and Lacabanne, C. (1972) *J. Polym. Sci.*, 11: 1631.
5. Lacabanne, C., Chatain, D.C., and Mompajens, J.C. (1977) *J. Macrom. Sci. Phys.*, B134: 537.
6. Lacabanne, C., Chatain, D.C., Mompajens, J.C., Hiltner, A., and Baer, E. (1978) *Solid State Commun*, 27: 1055.
7. Lacabanne, C., Chatain, D., Monpagens, J.C., and Berticat, P. (1979) *J. Appl. Phys.*, 50: 2723.

8. Lacabanne, C., Lamure, A., Teyssedre, G., Bernès, A., and Mourgues, M. (1994) *J. Non-Cryst. Solids*, 172–174: 884.
9. Crine, J.P. (1989) *J. Appl. Phys.*, 66: 1308.
10. McCrum, M.G. (1982) *Polymer*, 23: 1261.
11. McCrum, M.G. (1984) *Polymer*, 25: 299.
12. Peschanskaya, N.N., Yakushev, P.N., Sinani, A.B, and Bershtein, V.A. (1994) *Thermochim. Acta*, 238: 429.
13. Bershtein, V.A., Peschanskaya, N.N., Halary, J.L., and Monnerie, L. (1999) *Polymer*, 40: 6687.
14. Doulut, S., Demont, P., and Lacabanne, C. (2000) *Macromolecules*, 33: 3425.
15. Dufresne, A., Etienne, S., Perez, S., Demont, P., Diffalah, M., Lacabanne, C., and Martinez, J. (1996) *J. Polymer*, 37: 2359.
16. Martinez, J. and Lacabanne, C. (1993) *Thermochimica Acta*, 226: 51.
17. Lacabanne, C., Doulut, S., Bacharan, C., Demont, P., and Bernès, A. (1998) *J. Non-Cryst. Solids*, 235–237: 645.
18. Diffalah, M., Demont, Ph., and Lacabanne, C. (1993) *Thermochimica Acta*, 226: 33.
19. Migahed, M.D., Ahmed, M.T., and Kotp, A.E. (2000) *J. Phys. D: Appl. Phys.*, 33: 2108.
20. Boye, J., Martinez, J.J., Lacabanne, C., Perret, P., Chabert, B., and Gerard, J.F. (1992) *Polymer*, 33: 323.
21. Ponteins, P., Medda, B., Demont, P., Chatain, D., and Lacabanne, C. (1997) *Polym. Eng. Sci.*, 37: 1598.
22. Demont, P., Diffalah, M., Martinez-Vega, J.J., and Lacabanne, C. (1994) *J. Non-Cryst. Solids*, 172–174: 978.
23. Tang, H.H.Y. and Williams, H.L. (1990) *J. Appl. Polym. Sci.*, 40: 495.
24. Dufresne, A. and Lacabanne, C. (1995) *Polymer*, 36: 4417.
25. Ponteins, Ph., Medda, B., Demont, Ph., and Lacabanne, C. (1997) *J. Therm. Anal.*, 48: 623.
26. Cuesta Arenas, J.M., Mano, J.F., and Gomez Ribelles, J.L. (2002) *J. Non-Cryst Solids*, 307–310: 758.
27. Alves, N.M., Mano, J.F., and Gómez Ribelles, J.L. (2001) *Polymer*, 42: 4173.
28. Sauer, B.B., Avakian, P., Hsiao, B.S., and Starkweather, H.W. (1990) *Macromolecules*, 23: 5119.
29. Mano, J.F., Correia, N.T., and Moura Ramos, J. (1994) *J. Polymer*, 35: 3561.
30. Kattan, M., Cabot, C., Dargent, E., Bayard, J., and Grenet, J. (1998) *J Therm Anal*, 51: 765.
31. Ménégotto, J., Demont, Ph. , and Lacabanne, C. (2001) *Polymer*, 42: 4375.
32. Ménégotto, J., Demont, P., Bernes, A., and Lacabanne, C. (1999) *J Polym Sci, Part B: Polym Phys*, 37: 3494.
33. Nikonorova, N.A., Borisova, T.I., Barmatov, E.B., Pissis, P., and Diaz-Calleja, R. (2002) *Polymer*, 43: 2229.
34. Boye, J., Demont, P., and Lacabanne, C. (1994) *J. Polym. Sci., Part B: Polym. Phys.*, 32: 1359.
35. Alves, N.M., Mano, J.F., and Gómez Ribelles, J.L. (2002) *J. Therm. Analys. Calorim.*, 70: 633.
36. Alves, N.M., Mano, J.F., and Gómez Ribelles, J.L. (2001) *Mat. Res. Innovat.*, 4: 170.
37. Alves, N.M., Mano, J.F., and Gómez Ribelles, J.L. (2003) *Plast. Rubb. Process. Appl.*, 32: 281.
38. Alves, N.M., Mano, J.F., Gómez Ribelles, J.L., and Gómez Tejedor, J.A. (2004) *Macromolecules*, 37: 3735.
39. Alves, N.M, Senentxu, L.-M., Mano, J.F., and Gómez Ribelles, J.L. (2002) *Defects and Diffusion Forum*, 206–207: 131.
40. Alves, N.M., Mano, J.F., and Gómez Ribelles, J.L. (2002) *Polymer International*, 51: 434.
41. Bucci, C., Fieschi, R., and Guidi, G. (1966) *Phys. Rev.*, 148: 816.
42. Mano, J.F.. *Mater. Res. Innovat*, in press.
43. Carr, S.H. (1982. In *Electric Properties of Polymers*. Seanor, D.A. (ed.), Academic Press: New York.
44. Chen, R. and Haber, G. (1968) *A Chem. Phys. Lett.*, 2: 483.
45. Dargent, E., Kattan, M., Cabot, C., Lebaudy, P., Ledru, J., and Grenet, J. (1999) *J. Appl. Polym Sci.*, 74: 2716.

46. Ibar, J.P. (1997) *J. Macromol. Sci.- Rev. Macrom. Chem. Phys.*, C37: 389.
47. Sauer, B.B. and Avakian, P. (1992) *Polymer*, 33: 5128.
48. Dufresne, A., Lavergne, C., and Lacabanne, C. (1993) *Solid State Commun*, 88: 753.
49. Alves, N.M., Mano, J.F., and Gómez Ribelles, J.L. (1999) *Macromol. Symp.*, 148: 437.
50. Mano, J.F. (1998) *J Phys D: Appl Phys*, 31: 2898.
51. Mano, J.F. (2000) *J Phys D: Appl. Phys.*, 33: 280.
52. Satoto, R., Morikawa, J., and Hashimoto, T. (1999) *Polym. Int.*, 48: 509.
53. Fahmy, T. and Ahmed, M.T. (2000) *Polym. Int.*, 49: 669.
54. Bernes, A., Chatain, D., and Lacabanne, C. (1992) *IEEE Transactions on Electrical Insulation*, 27: 464.
55. Sauer, B. and Moura Ramos, J. (1997) *Polymer*, 38: 4065.
56. Doulut, S., Becharan, C., Demont, P., Bernès, A., and Lacabanne, C. (1998) *J. Non-Cryst. Solids*, 235–237: 645.
57. Mano, J.F. and Moura Ramos, J.J. (1995) *J. Thermal Analysis*, 44: 1037.
58. Dudognon, E., Bernès, A., and Lacabanne, C. (2001) *Macromolecules*, 34: 3988.
59. Dudognon, E., Bernès, A., and Lacabanne, C. (2002) *Macromolecules*, 35: 5927.
60. Marchal, E. (1992) *J. Chem. Phys.*, 96: 4676.
61. Marchal, E. (1994) *J. Non-Cryst. Solids*, 172–174: 902.
62. Teyssèdre, G. (1993) PhD Thesis, Toulouse.
63. Ronarc'h, D., Audren, P., and Moura, J.L. (1985) *J Appl Phys*, 58: 474.
64. Peacock-Lopez, E. and Suhl, H. (1982) *Phys. Rev.*, B26: 3774.
65. Moura Ramos, J.J., Mano, J.F., and Sauer, B.B. (1997) *Polymer*, 38: 1081.
66. (a) Mialhe, P.. *J.Phys. D, Appl. Phys.*, 1989, 22: 720; (b) Krug, R.R., Hunter, W.G., and Grieger, R.A. (1976) *Nature*, 261: 566.
67. Mano, J.F., Correia, N.T., Moura-Ramos, J.J., Andrews, S.R., and Williams, G. (1996) *Liq. Crystals*, 20: 201.
68. Zielinski, M., Swiderski, T., and Kryszewski, M. (1978) *Polymer*, 19: 882.
69. Read, B.E. (1989) *Polymer*, 30: 1439.
70. Alves, N.M., Mano, J.F., and Gómez Ribelles, J.L. (2002) *Polymer*, 43: 3627.
71. Dobbertin, J., Hensel, A., and Schick, C. (1996) *J. Thermal Analysis*, 47: 1027.
72. Struik, L.C.E. (1987) *Polymer*, 28: 1521.
73. Shick, C., Kramer, L., and Mischok, W. (1985) *Acta Polym.*, 36: 47.
74. Struik, L.C.E. (1978) *Physical Ageing in Amorphous Polymers and other Materials*. Elsevier Science: Amsterdam.
75. Diego, J.A., Cañadas, J.C., Mudarra, M., and Belana, J. (1999) *Polymer*, 40: 5355.
76. Zhao, J., Song, R., Zhang, Z., Linghu, X., Zheng, Z., and Fan, Q. (2001) *Macromolecules*, 30: 343.
77. Ward, I.M. and Hadley, D.W. (1993) *An Introduction to the Mechanical Properties of Solid Polymers*. John Wiley & Sons: New York.
78. Aklonis, W.L. and McKnight, W.J. (1983) *Introduction to Polymer Viscoelasticity*. John Wiley & Sons: New York.
79. Dargent, E., Grenet, J., and Dahoun, A. (1997) *Polym. Eng. Sci.*, 37: 1853.
80. Mano, J.F., Moura Ramos, J.J., Fernandes, A., and Williams, G. (1994) *Polymer*, 35: 5170.
81. Kattan, M., Dargent, E., and Grenet, J. (2002) *Polymer*, 43: 1399.
82. Adam, G. and Gibbs, J.H. (1965) *J. Chem. Phys.*, 43: 139.
83. Saito, S. and Nakajima, T. (1959) *J. Appl. Polym. Sci.*, 2: 93.
84. Mano, J.F., Alves, N.M., Meseguer Dueñas, J.M., and Gómez Ribelles, J.L. (1999) *Polymer*, 40: 6545.
85. Sauer, B.B and Kim, Y.H. (1997) *Macromolecules*, 30: 3323.
86. Matsuoka, S. (1992) *Relaxation Phenomena in Polymers*. Hanser: Munich.
87. Ngai, K.L. and Rendell, R.W. (1991) *J. Non-Cryst. Solids*, 131–133: 942.
88. Kramarenko, V.Y., Ezquerra, T.A., Sics, I., Baltá-Calleja, F.J., and Privalko, V.P. (2000) *J. Chem. Phys.*, 113: 447.

89. Casalini, R., Fioretto, D., Livi, A., Lucchesi, M., and Rolla, P.A. (1997) *Phys. Rev. B*, 56: 3016.
90. Glatz-Reichenbach, J.K.W., Sorriero, L.J., and Fitzgerald, J.J. (1994) *Macromolecules*, 27: 1338.
91. Prochazka, F., Durand, D., and Nicolai, T.J. (1999) *Rheol.*, 43: 1511.
92. Perez, J., Muzeau, E., and Cavaillé, J.Y. (1992) *Plast. Rubb. Compos. Applic.*, 18: 139.
93. Hempel, E., Beiner, M., Huth, H., and Donth, E. (2002) *Thermochimica Acta*, 391: 219.
94. Mudarra, M., Joumha, A., Belana, J., and Toureille, A. (1999) *Polymer*, 40: 6977.
95. Gourari, A., Bendaoud, M., Lacabanne, C., and Boyer, R.F. (1985) *J. Polym. Sci., Polym. Phys. Ed.*, 23: 889.
96. Lacabanne, C. and Chatain, D. (1973) *J. Polym. Sci., Polym. Phys. Ed.*, 11: 2315.
97. Alegria, A., Guerrica-Echevarria, E., Telleria, I., and Colmenero, J. (1993) *Phys. Rev. B*, 47: 14857.
98. (a) Startkweather, H.W. *Macromolecules*, (1981), 14: 1277; (b) Sauer, B.B., Avakian, P., Startkweather, H.W. (1990) *Macromolecules*, 23: 5119; (c) Startkweather, H.W. (1991) *Macromolecules*, 21: 1798.
99. Mano, J.F. (1999) *Thermochim. Acta*, 332: 161.
100. Mano, J.F. and Saiter, J.M.. *Colloid & Polymer Science*, accepted.
101. Mudarra, M., Belana, J., Cañadas, J.C., and Diego, J. (1999) *A Polymer*, 40: 2659.
102. Alves, N.M., Mano, J.F., Gómez Ribelles, J.L., and Gómez Tejedor, J. (2004) *A Polymer*, 45: 1007.
103. Alves, N.M., Mano, J.F., Balaguer, E., Meseguer Dueñas, J.M., and Gómez Ribelles, J.L. (2002) *Polymer*, 43: 4111.